npj | climate and atmospheric science

Article

Published in partnership with CECCR at King Abdulaziz University

https://doi.org/10.1038/s41612-025-01063-3

Deciphering the capricious precipitation response: irrigation impact in the North China Plain

Yuwen Fan[1] ✉, Zhao Yang[2], Min-Hui Lo[3], Jina Hur[4] & Eun-Soon Im[1,5] ✉

Intensive irrigation in the North China Plain (NCP) raises environmental concerns, yet its climate impacts remain inconsistent among current modeling studies. These inconsistencies may arise from deficiencies in existing models. To better capture irrigation impact, we employed a recently improved irrigation model tailored for the NCP, which significantly enhances simulations of crop growth and irrigation application. Results reveal that irrigation exerts competing effects on precipitation: enhancing it in May and June by increasing rainfall frequency and intensity, while suppressing it in July and August by reducing intensity. Spatial precipitation changes correlate with upper-tropospheric humidity, while inter-annual changes link to geopotential height and wind anomalies. This suggests that irrigation-induced surface cooling and moisturizing modulate atmospheric thermodynamic and dynamic structures, influencing convective precipitation unevenly across regions and time, leading to complex precipitation changes. These findings highlight the complexity of irrigation impacts and emphasize the need for improved land representation in climate models.

Irrigation, as a crucial agricultural practice, plays a vital role in ensuring food security and sustaining agricultural productivity[1,2]. Unsurprisingly, the intensive and extensive water consumption for irrigation has raised concerns about its potential impact on the climate system, particularly in regions like the North China Plain (NCP). As one of the largest plains in eastern China (highlighted by the red box in Fig. 1), the NCP features low elevations (mostly below 100 m), which support its suitability for cultivation. This region is predominantly covered by cropland, with a significant portion dedicated to double-cropping systems[3] (Fig. 1b). Despite the extensive cropland coverage, the climatological precipitation in the NCP is only about half of that in southern China[4] (Fig. 1c), highlighting the critical reliance for irrigation. According to the FAO AQUASTAT database[5], irrigated cropland accounted for more than 70% of the total land use in the region's pluvial areas in 2005 (Fig. 1d).

All these unique characteristics make the NCP particularly vulnerable to irrigation. However, the irrigation climate impact in NCP is still debatable among the existing literature. While most studies acknowledge that irrigation has resulted in significant cooling[6–11] and an increase in spring precipitation[7,9,11,12], the effects on summer precipitation remain far less clear. Specifically, the regional climate model (RCM)-based studies have reported conflicting results, with some suggesting that irrigation promotes summer precipitation[8,10,12], while others suggest a reduction[6,9]. Meanwhile, some studies argue that the summer precipitation changes are heterogeneous, varying across different areas in eastern China[7,11]. This divergence in findings is particularly significant because summer precipitation is the main source of rainfall in the NCP, accounting for the majority of the annual total[13]. The ongoing uncertainty regarding how irrigation influences summer precipitation underscores the complexity of its overall impact on the regional climate system.

The inconsistency and heterogeneity in the existing literature can be attributed to inherent differences in climate models and the lower sensitivity of summer precipitation to additional moisture compared to the drier spring season. However, the limited capabilities of current crop and irrigation models[14,15] are more likely the primary reason for these inconsistencies.

First, these models may not fully account for dynamic vegetation, as they struggle to accurately simulate irrigated vegetation patterns and their sensitivity to water availability. Most studies simply add water to soil surface while adopting the same satellite-defined vegetation in both irrigation and non-irrigation scenarios, thereby neglecting the indirect effects of irrigation through vegetation promotion. Given that vegetation can account for a substantial portion of the biosphere and atmosphere interactions[16], typically the precipitation[17–19], this oversight can lead to considerable

[1]Division of Environment and Sustainability, The Hong Kong University of Science and Technology, Hong Kong, China. [2]Pacific Northwest National Laboratory, Richland, WA, USA. [3]Department of Atmospheric Sciences, National Taiwan University, Taipei, Taiwan, ROC. [4]National Institute of Agricultural Sciences, Rural Development Administration, Wanju-gun, Jeollabuk-do, Korea. [5]Department of Civil and Environmental Engineering, The Hong Kong University of Science and Technology, Hong Kong, China. ✉e-mail: yfanaj@connect.ust.hk; ceim@ust.hk

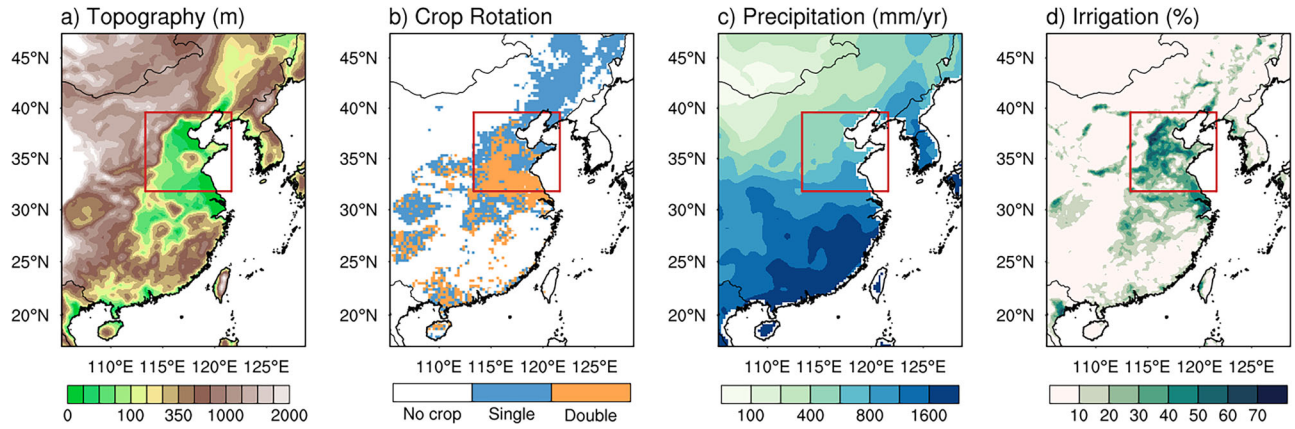

Fig. 1 | Basic information about the NCP region. a Topography (m), **b** Crop Rotation, **c** Annual Precipitation (mm/yr), **d** Fraction of irrigation (%) over the model domain, where the red box highlights the NCP region.

misrepresentation of the irrigation impact. Wu et al.[7] highlighted that neglecting dynamic vegetation could lead to an approximate 30% underestimation of irrigation impacts. Similarly, Harding et al.[20] also demonstrated that utilizing dynamic irrigated crops results in greater precipitation increases compared to static crops.

Second, the crop and irrigation seasons are often misrepresented. The NCP widely employs a distinctive double-cropping rotation, as evident from satellite vegetation patterns[3,21], which is rarely considered in current climate models. Consequently, many models are only activated for the summer crop, overlooking the winter and early spring irrigation. This omission can lead to skewed conclusions since the dry season, particularly early spring, might be more sensitive to irrigation and could have a more pronounced impact on the local climate[11]. Liu et al.[9] also claim that spring irrigation may decrease summer precipitation due to the long memory of soil moisture. Although a few studies attempt to incorporate double-cropping or winter irrigation by predefining the crop season[6,7,9], this predefined approach may fail to capture the slower growing degree day (GDD) accumulation and affected growth rates due to irrigation-induced cooling[9,22].

Third, the simulation of crop growth and irrigation amounts can be imprecise. Models using default schemes calibrated with global or U.S. data may not accurately reflect the spatial and temporal variability of conditions in the NCP. Given that irrigation responses are highly region-specific, it is crucial to regionalize these models to capture more localized details, which has been shown to significantly improve the simulation of crop growth and irrigation[22–24].

These limitations constrain a comprehensive understanding of irrigation-induced climate effects. To address these challenges, we adopted a recently developed integrated irrigation model specifically tailored to the NCP[22]. This model is built upon the Noah land surface model with multi-parameterization options (Noah-MP) and is coupled with the Weather Research and Forecasting Model (WRF), previously used to study the irrigated agriculture inside the United States. To make it more applicable to the NCP, which has totally different conditions from the United States, Fan et al.[22] have recalibrated the parameters using local data and incorporated several new features, including dynamic crop growth, multiple crop seasons, and interactive irrigation applications. These modifications enable the simulation of double cropping rotation and cold season irrigation, both of which are critical to NCP but were previously omitted in earlier versions of the model. Additionally, the improved model captures how crops respond dynamically to various irrigation levels, enabling two-way feedback between irrigated crops and the climate. Overall, the improved model effectively addresses the three limitations mentioned earlier, which can be evident in the model's enhanced ability to simulate crop stages, field biomass and monthly leaf area index (LAI), as well as capture the regional differences in irrigation application. However, these model advancements have primarily focused on land surface variables and have not yet been applied to evaluate atmospheric or hydrological processes. Thus, our study aims to adopt this improved model to systematically investigate the irrigation impacts on regional climate. To ensure the reliability of our findings, we first evaluate the model's performance in simulating climate-related variables. Then, we analyze the spatial and temporal patterns of temperature and precipitation changes to better understand their seasonal variations and their underlying mechanisms. By exploring the complex relationship between irrigation practices and climate, this study seeks to provide insights that can inform more effective and sustainable water resource management strategies in the context of a changing climate.

Results

Validation

Given the interactions between the atmosphere and irrigated crops, we conduct validation on six key variables from background climate (temperature and precipitation), vegetation pattern (LAI and grain mass), and hydrological sectors (irrigation application and total runoff). The purpose of this validation is to ensure that the model accurately captures the overall ecohydrological cycle, and the inclusion of irrigation improves the model's performance in simulating irrigation-related variables. Therefore, we validate both the spatial climatology patterns (Fig. 2) and the temporal patterns, including inter and intra-annual variability (Fig. 3). Note that both the control experiment (CTL, scenario without irrigation) and the irrigation experiment (IRR, scenario with irrigation) are conducted using the improved model. The unimproved model was excluded from the validation process, as it may not be capable of reasonably predicting yield or irrigation amounts[22].

Figure 2 shows the spatial validation in the focused NCP region only, while the validation for the whole model domain over eastern China is provided as Fig. S1. IRR performs much better across most variables, especially for vegetation growth and runoff. Notably, irrigation-induced cooling shifts the warm bias to a cold bias, but with a smaller magnitude. Figure 3 displays the monthly and yearly average temperatures over the NCP land. Although CTL only shows a slight systematic cold bias in the yearly average (Fig. 3b), there is actually a pronounced warm bias from April to September (when the crop grows better based on Fig. 3c), partially offsetting the cold bias observed in winter, as shown by the orange bars in Fig. 3a. Irrigation significantly reduces the summer warm bias, thus, leading to a more pronounced net cold bias in the annual average (blue bars in Fig. 3a, b). Given that our primary focus is on the crop season, the winter cold bias may have a smaller impact on our conclusions, and the temperature in Fig. 2 is only validated from April to September. The benefit of incorporating irrigation to reduce the warm bias is also found in central US[25].

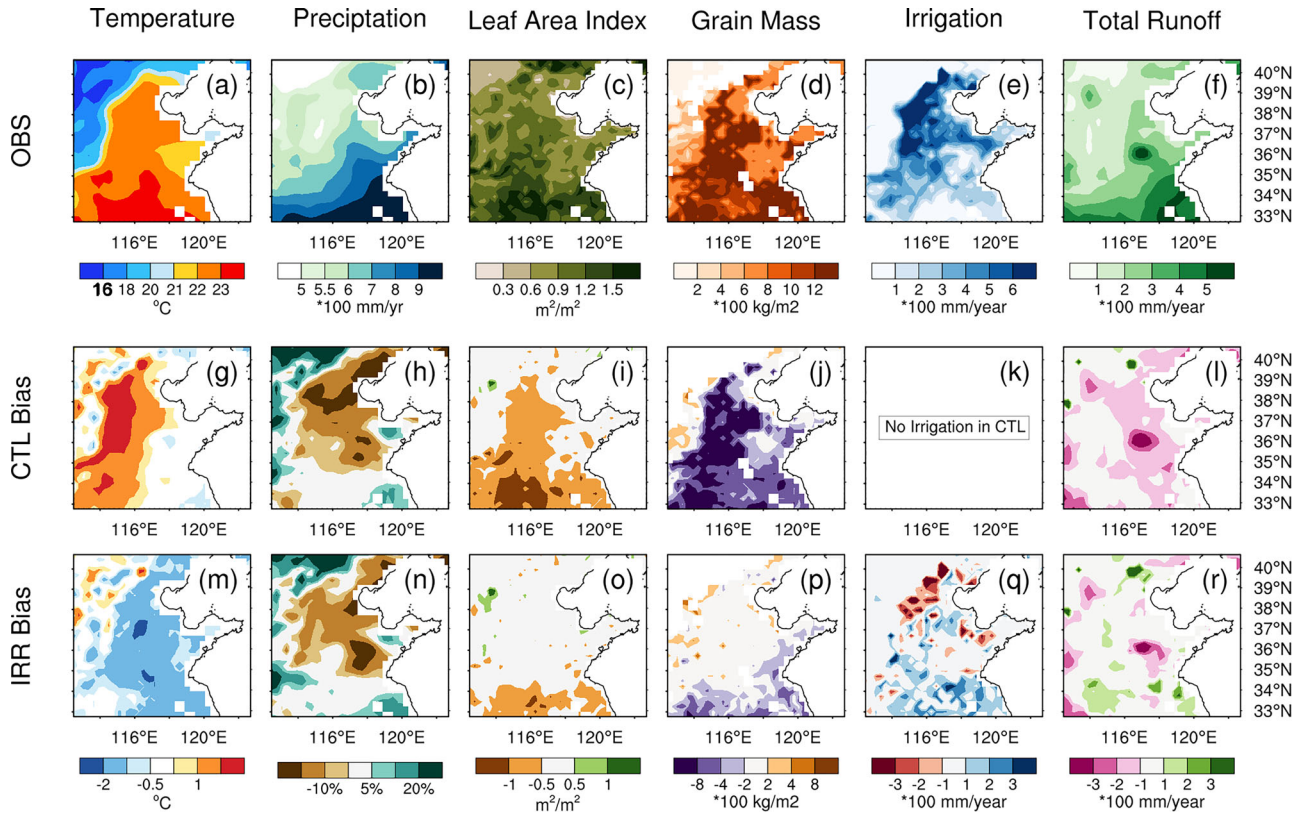

Fig. 2 | Spatial validation for climatology annual mean of the CTL and IRR simulation in 2005-2014 for NCP region only. a–f Mean of OBS. **g–l** Bias of CTL (i.e., CTL-OBS). **m–r** Bias of and IRR (i.e., IRR-OBS). Temperature validation is conducted for crop season (Apr–Sep) only. Grain mass and irrigation are only shown in the crop area, with non-cropping areas being masked out.

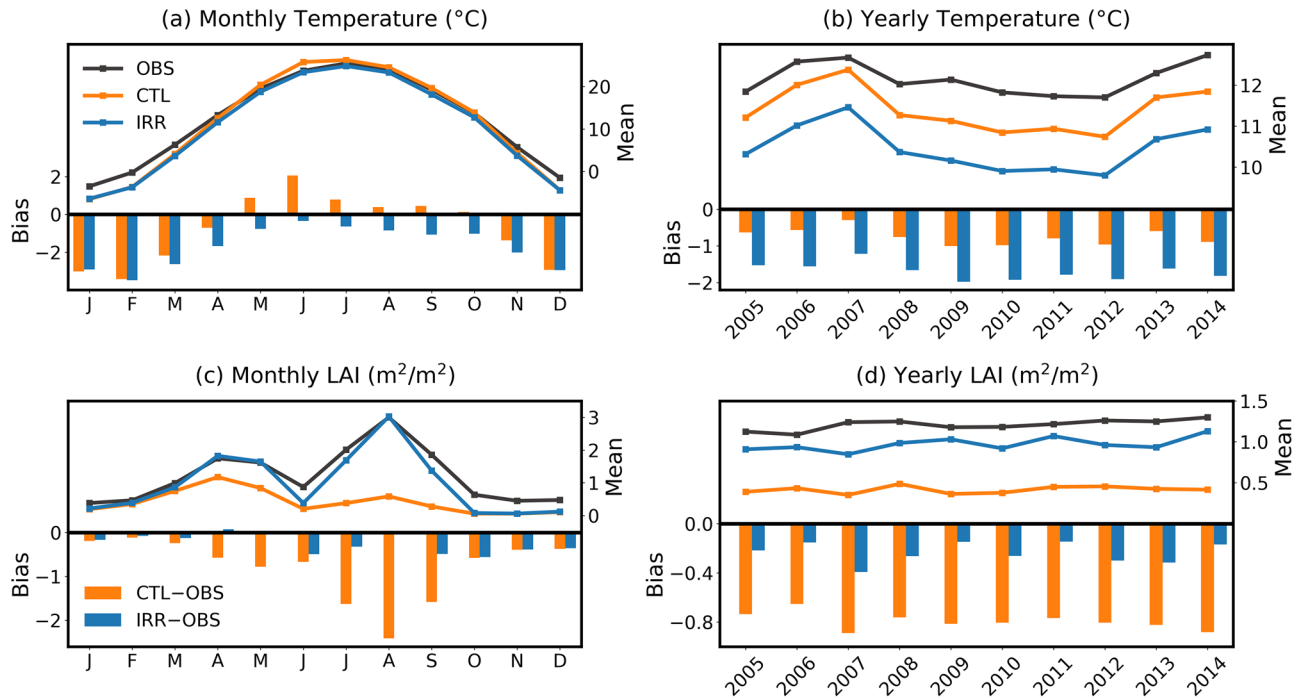

Fig. 3 | Temporal validation for the CTL and IRR simulation in 2005-2014. Lines represent the spatially averaged value of both observation and simulations, while the bars represent the bias of each simulation compared with the observations shown in the lines. Black, orange and blue represent OBS, CTL and IRR, respectively. **a** Monthly temperature over the NCP region. **b** Yearly temperature over the NCP region. **c** Monthly LAI over the double-cropping area in the NCP region. **d** Yearly LAI over the double-cropping area in the NCP region.

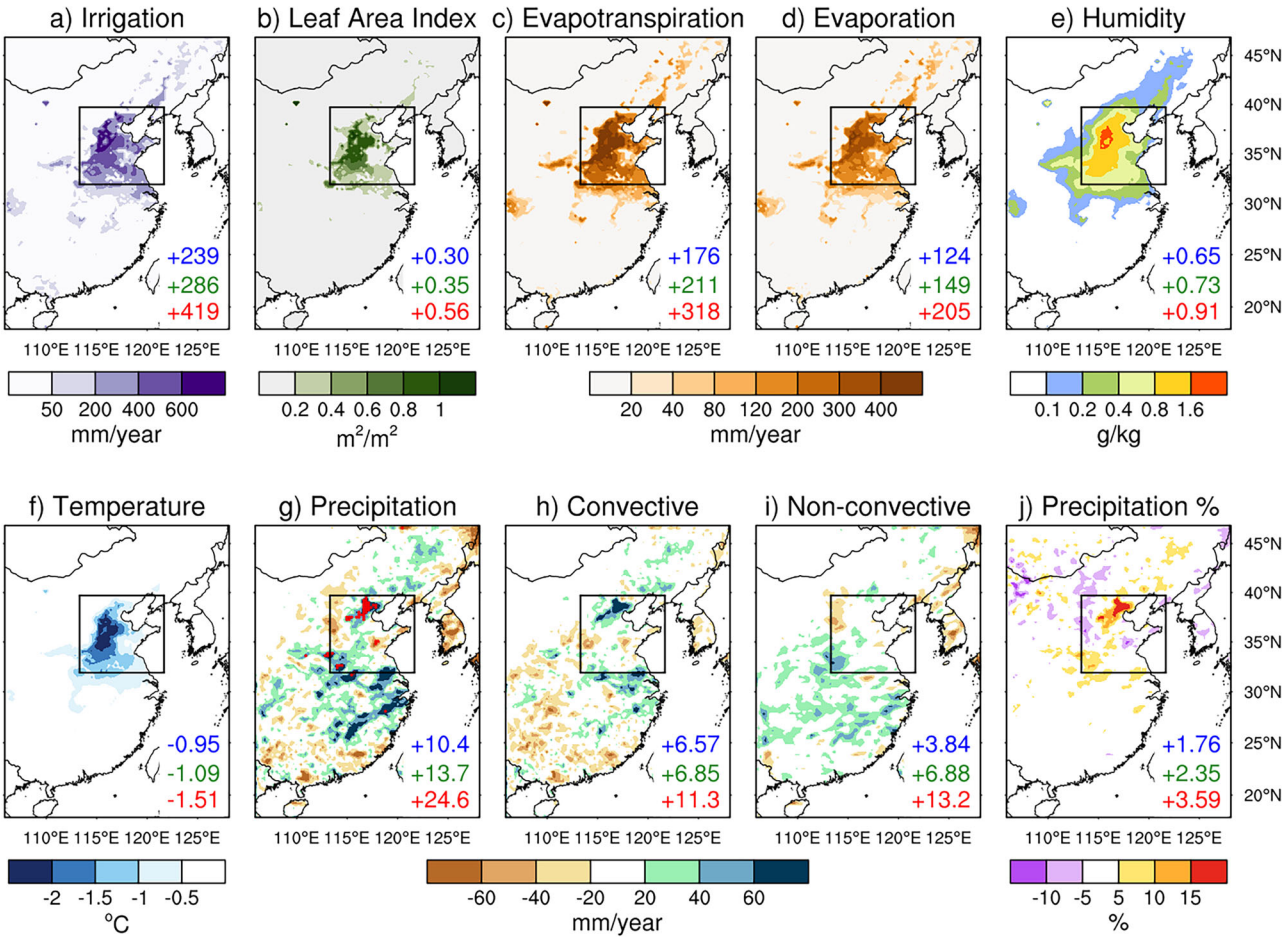

Fig. 4 | Irrigation amount and its annual impact. a Climatology mean of irrigation amount (mm/yr) and **b**–**j** irrigation-induced changes (IRR−CTL) in climatology mean of **b** leaf area index (m^2/m^2), **c** evapotranspiration (mm/yr), **d** ground evaporation (mm/day), **e** 2 m humidity (g/kg), **f** 2 m temperature (°C), **g** total precipitation (mm/yr), (h) convective precipitation (mm/yr), **i** non-convective precipitation (mm/yr), and **j** relative precipitation changes (%). The red-colored regions in **g** total precipitation highlight the regions that meet the following criteria: (1) precipitation changes consistently increase or decrease for at least 7 out of the 10 years analyzed, (2) the absolute annual change (either increase or decrease) exceeds 50 mm, (3) the relative annual change (either increase or decrease) exceeds 10%, and (4) the annual changes are statistically significant at the 95% confidence level as determined by a t-test. The numbers indicate spatial mean changes over NCP land grids (blue), crop grids (green), and double-cropping grids (red).

Additionally, the IRR simulation shows a markedly improved ability to reproduce vegetation or crop growth, typically in double-cropping regions. Fig. S2 displays monthly averages over land, cropland (excluding mountainous regions), single-cropping regions, and double-cropping regions, separately. IRR significantly enhances model predictability in the heavily irrigated double-cropping region (Fig. 3c or Fig. S2h). However, in the single-cropping region, it overestimates the LAI during the growing season and shows no changes during the non-growing season (Fig. S2f), resulting in an overall yearly mean LAI that remains below observed values (Fig. 3d). Nevertheless, the overall improvement compared to CTL underscores the critical role of irrigation in the double-cropping-dominant NCP. Since LAI is essential for modeling land-atmosphere interactions and energy partitioning[26,27], the substantial LAI gap between CTL and IRR also suggests that failing to incorporate vegetation responses can result in noticeable deviations when quantifying the irrigation impact.

General irrigation impact on climatology

The validation of both spatial and temporal patterns for selected variables confirms the reliability of our simulations in studying the impacts of irrigation. Based on this validation, Fig. 4a presents the average irrigation amount from 2005 to 2014, while Fig. 4b-j display the climatological differences in climate variables between irrigation and non-irrigation experiments (i.e., IRR−CTL). As expected, irrigation is primarily concentrated in the NCP region, directly promoting vegetation growth, especially in double-cropping areas. The additional water and enhanced vegetation lead to greater evapotranspiration, driven primarily by increased evaporation from wetter soil conditions and, to a lesser extent, by transpiration from more vigorous vegetation. This further leads to localized cooling in the near-surface atmosphere, with the most significant cooling of ~2 °C and an average of about 1 °C over the NCP region. Furthermore, a substantial increase in humidity, approximately 0.0016 kg/kg or around 30%, occurs exactly where intensive irrigation and cooling are observed. All these changes are uniform across the region, with their magnitude corresponding to the spatial distribution of irrigation.

As mentioned previously, precipitation changes are more heterogeneous. Our findings indicate that while humidification favors precipitation, it occurs simultaneously with cooling-induced stabilization which is less favorable for precipitation. Nevertheless, we found notable increases in convective precipitation exist in the northern NCP and to the south of it, as well as a less pronounced increase in non-convective precipitation in almost the whole southern China. Although decreases in both convective and non-convective precipitation can be observed, they are neither significant nor consistently happen in each year when considering total precipitation changes. Thus, only a few areas show statistically significant and consistent precipitation increases that meet the following criteria: (1) precipitation changes consistently increase or decrease for equals to or more than 7 out of

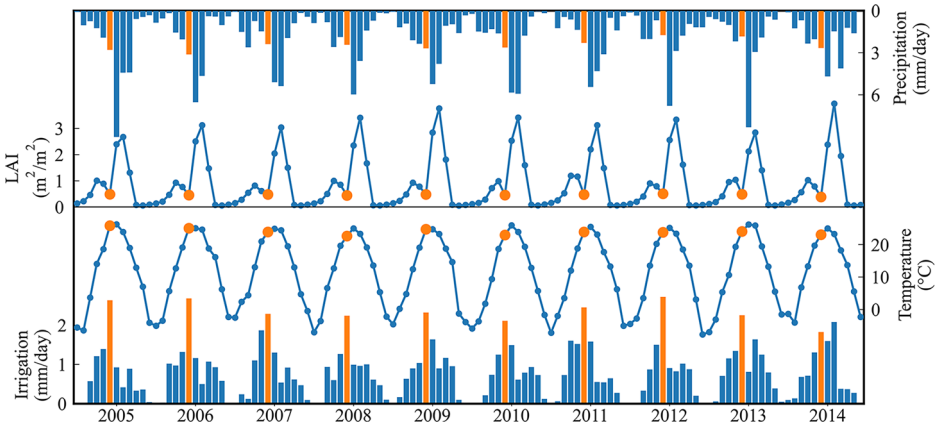

Fig. 5 | Monthly patterns of IRR over NCP croplands. From bottom to top: irrigation (mm/day), 2-m temperature (°C), LAI (m^2/m^2), and precipitation (mm/day). June is highlighted in orange as a special case.

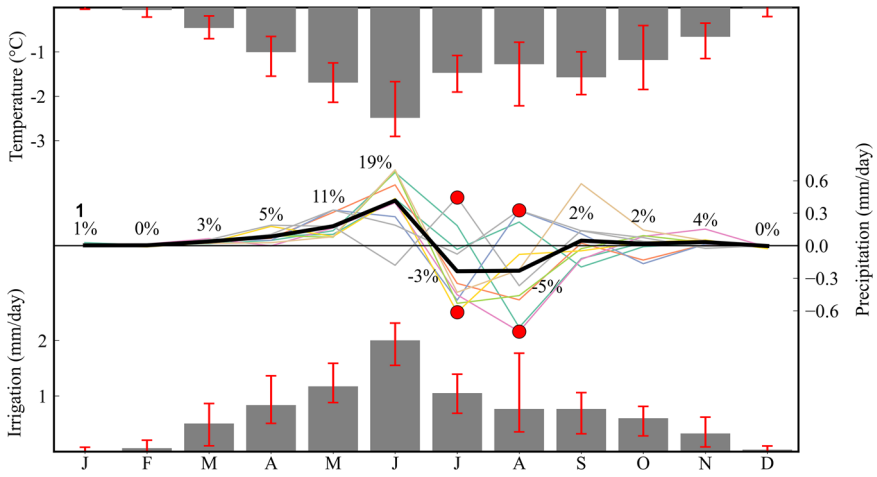

Fig. 6 | Monthly averages of IRR irrigation (bars in the bottom), irrigation-induced changes (IRR −CTL) in 2 m temperature (bars at top), and precipitation changes (lines in the middle) averaged over 10 years for the whole NCP. Red error bars on the box plots indicate the inter-annual range over 10 years. Colorful lines represent precipitation changes in different years, while the thick black line shows the 10-year average. Numbers along the line indicate relative changes compared to monthly precipitation in the CTL experiment. Red dots highlight extreme months selected for analysis in Section 3.4.

the 10 years analyzed, (2) the absolute annual change (either increase or decrease) exceeds 50 mm, (3) the relative annual change (either increase or decrease) exceeds 10%, and (4) the annual changes pass the 95% confidence interval as determined by a statistical t-test. These regions with significant and consistent annual increases also experience a notable rise in convective precipitation, particularly in parts of northern NCP, where these changes contribute to over 15% of the annual precipitation. In contrast, while precipitation increases in southern China are significant and consistent, they typically account for less than 5% of the annual total (Fig. 4j), thus not highlighted in Fig. 4g.

Temporal pattern of irrigation, temperature and precipitation

The feedback between irrigation and local climate is bidirectional. Thus, we first examine how seasonal patterns of climate and vegetation influence the irrigation simulation, and then explore the reverse relationship, analyzing how climate, typically temperature and precipitation, respond to irrigation practices.

Figure 5 illustrates the monthly averages of irrigation, temperature, LAI, and precipitation across the NCP cropland, arranged from bottom to top in the figure. June exhibits the highest irrigation intensity, as indicated by the orange highlighting, coinciding with elevated temperatures, reduced LAI, and comparatively low precipitation. The relatively high temperatures in June accelerate evapotranspiration, while low LAI indicates little vegetation cover and spacious exposed barelands, further enhancing evaporative losses. Simultaneously, the precipitation remains significantly below the July-August rainy season and only provides limited water supplement. These conditions contribute to soil moisture deficit collectively, thereby intensifying irrigation requirements. Several studies also notice this irrigation peak in pre-summer, albeit with some discrepancies regarding the precise timing of it. Some studies identify May as the peak[7,11], while Yang et al.[6] suggests June. These variations can be attributed to differences in vegetation simulation. For instance, the single-cropping simulation in Fan et al.[11] potentially overlooks the LAI reduction in June and underestimates irrigation demands during the crop transition (i.e., after winter wheat harvest and before summer corn seeding). This also underscores the importance of implementing double-cropping functions in assessing irrigation impacts. Furthermore, even with double-cropping rotation, our simulations focus solely on the winter wheat and summer maize rotation, which may not accurately represent other cropping patterns (i.e., three crops in two years or single annual crops) that do not follow the same transition timeline as our cropping rotation. The potential underestimation of vegetation cover in June could lead to an exaggerated simulation of bare-land evaporation loss and irrigation demands. Further refinement in modeling approaches can be conducted to reduce the uncertainty.

With an understanding of how climate shapes the temporal patterns of irrigation demand, we now shift our focus to how irrigation influences climate patterns in the NCP region (Fig. 6). The lower boxes represent irrigation amount, while the upper ones depict changes in 2-m temperature, both with red error bars indicate the range of monthly variations over the 10-year period. Temperature reduction generally corresponds to irrigation intensity proportionally, with the greatest cooling effect observed in June, reaching ~2.5 °C (compared to an annual mean of 0.95 °C), coinciding with peak irrigation. This cooling effect aligns with findings from Liu et al.[9] and Fan et al.[11], both reporting maximum cooling of 2.5 °C and 2 °C, respectively, as well as Wu et al.[7], which noted a range of 1.2–2.6 °C, all reflecting similar water forcings during the hot season. Also, it is slightly stronger than

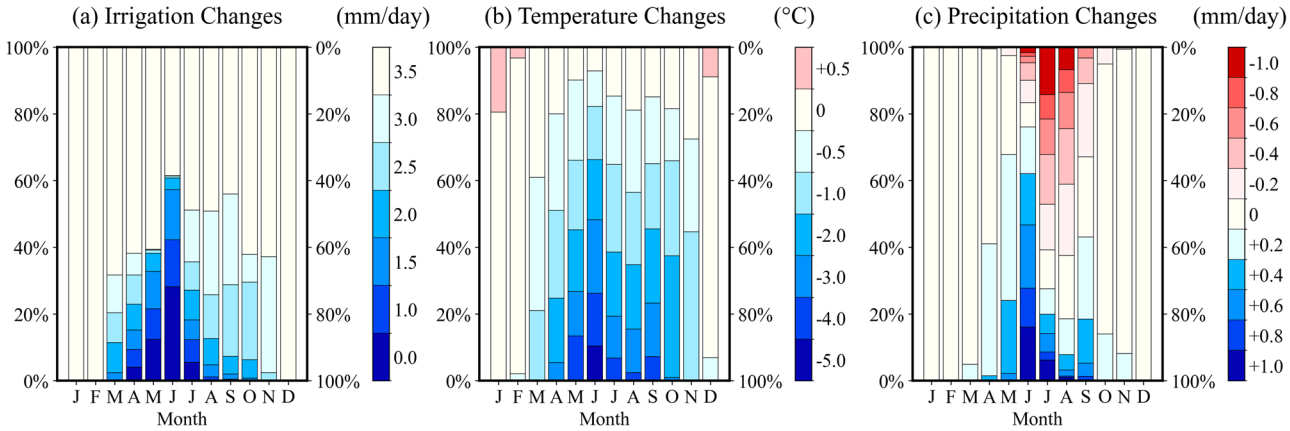

Fig. 7 | Monthly stacked frequency distributions of irrigation, and the induced changes on temperature, and precipitation over NCP grids between irrigated and control simulation (IRR−CTL). a Monthly irrigation amount (mm/day) **b** temperature changes (°C), and **c** precipitation changes (mm/day).

the mean cooling of 0.5 °C and a maximum of 2 °C reported by Wang et al.[28], and more pronounced than the 0.43 °C observed by Yuan et al.[29] without dynamic vegetation, and 0.23 °C from Yang et al.[6] with smaller water forcings. However, it remains weaker than the 1–4 °C cooling reported by Kang and Eltahir[8], which involved exaggerated water forcings. As shown in Fig. 2, 3, this cooling effect helps mitigate the significant warm bias observed in the NCP without irrigation, a finding consistent with other studies[11,28,29].

The central lines represent precipitation changes, with individual years depicted in various colors and the mean is shown as a thick black line. Percentages along the line indicate relative changes compared to the monthly precipitation of CTL experiment. Significant increases in precipitation are observed in May and June, which is also found in Wu et al.[7] and Fan et al.[11]. Conversely, there is a noticeable decrease in precipitation during July and August; however, this decline accounts for at most 5% of total rainfall since this is the rainy season. From a different perspective, the increases in precipitation during May and June exhibit a consistent pattern across the years, whereas July and August show great variability. This suggests that the precipitation increases in May and June are both statistically significant and consistent, while the decreases in July and August, despite their substantial absolute values, lack consistency and relative significance. The large variability in summer precipitation may be attributed to the greater inter-annual variability of irrigation practices as well as the more complex background atmospheric conditions[30], which will be discussed further in later sections.

Competition between precipitation enhancement and suppression

Although the average precipitation changes are not directly proportional to irrigation forcing, an analysis of grid distribution reveals a strong correlation (Fig. 7). Overall, the cooling is widespread, with ~80% of the grids experiencing a cooling of 0.5 °C or more from April to October. Precipitation increases are most pronounced in June, with over 60% of the grids showing an increase of 0.4 mm/day or more; and nearly 20% of the grids experience even greater increases of 1 mm/day or more. However, some grids also experience decreases, particularly in July and August, which compete with the increases, resulting in a lack of proportionality in the averaged trends. This competition between promotion and inhibition has been found in many literatures, and it can be attributed to several factors. For example, irrigation introduces additional moisture into the atmosphere, thereby increasing humidity and triggering precipitation[8,20,31,32]. Surface cooling also occurs during evaporation, which decreases the planetary boundary layer height and induces cyclonic anomalies at low levels and anticyclonic anomalies at high levels, thus inhibiting rainfall[33–35]. Additionally, changes in large-scale circulation may interact with prevailing background wind, potentially triggering new precipitation[33] or slowing moisture transport from the ocean to reduce precipitable water[36–40]. All these examples indicate that irrigation can enhance or suppress precipitation in many ways, and it is theoretically possible that both enhancement and suppression happen in the same region.

By showing how many grids in the NCP are experiencing precipitation increase or decrease, Fig. 7c serves as an excellent illustration of the counterbalance between the competing "enhancement" and "suppression". During spring and autumn, most of the grids encounter precipitation enhancement, leading to a large-scale and monotonic response that is proportional to irrigation forcing. In contrast, during summer, the suppression becomes more pronounced, countering and even slightly surpassing the enhancement, resulting in an overall insignificant signal. In the following section, we will further explore this competition from multiple perspectives.

Two indicators are utilized to explain the precipitation changes, CAPE (maximum daily convective available potential energy) which represents the thermodynamic 'enhancement' of precipitation due to moistening, and MADV (integrated dynamic term of vertical moisture advection[41,42]), which reflects the dynamical 'suppression' of precipitation caused by cooling stabilization. Fan et al.[11] found that CAPE increase outweighs MADV changes, thereby explaining the precipitation rise as a result of dominant thermodynamic moistening. Following them, we analyze the CAPE and MADV across land grids in the NCP for May–June (when precipitation increases) and July-August (when precipitation decreases) in Fig. 8. We notice a relatively higher CAPE and more negative MADV in July and August even without irrigation, indicating greater energy and moisture convergence (Fig. 8a, e). This corresponds to the fact that July and August account for most of the annual precipitation (Fig. 5). In the absence of irrigation, May and June show relatively low CAPE levels; however, irrigation significantly increases CAPE without causing substantial changes to MADV, resulting in many orange dots representing higher CAPE than the green dots, consistent with the results from Fan et al.[11]. On the other hand, even without irrigation, July and August already demonstrate very high CAPE, and the CAPE increase due to irrigation is minimal, so the overall CAPE pattern remains largely unchanged. In essence, CAPE does not vary significantly in July and August.

The second and third columns depict the daily precipitation across the whole 10-year period in both CTL and IRR experiments, with color representing the CAPE changes in Fig. 8b, f and MADV changes in Fig. 8c, g. In May and June, most dots are prominently red and positioned above the diagonal, indicating that precipitation increases occur in most grids and years, which correlates with significant CAPE increases found in the first column. Additionally, a cluster of red dots locates next to the y-axis, suggesting potential new rainfall events. This observation is further supported by the upward shift in the frequency distribution (Fig. 8d, h). In contrast, during July and August, CAPE increases are confined to the lower left corner, where light precipitation occurs, and CAPE even decreases with

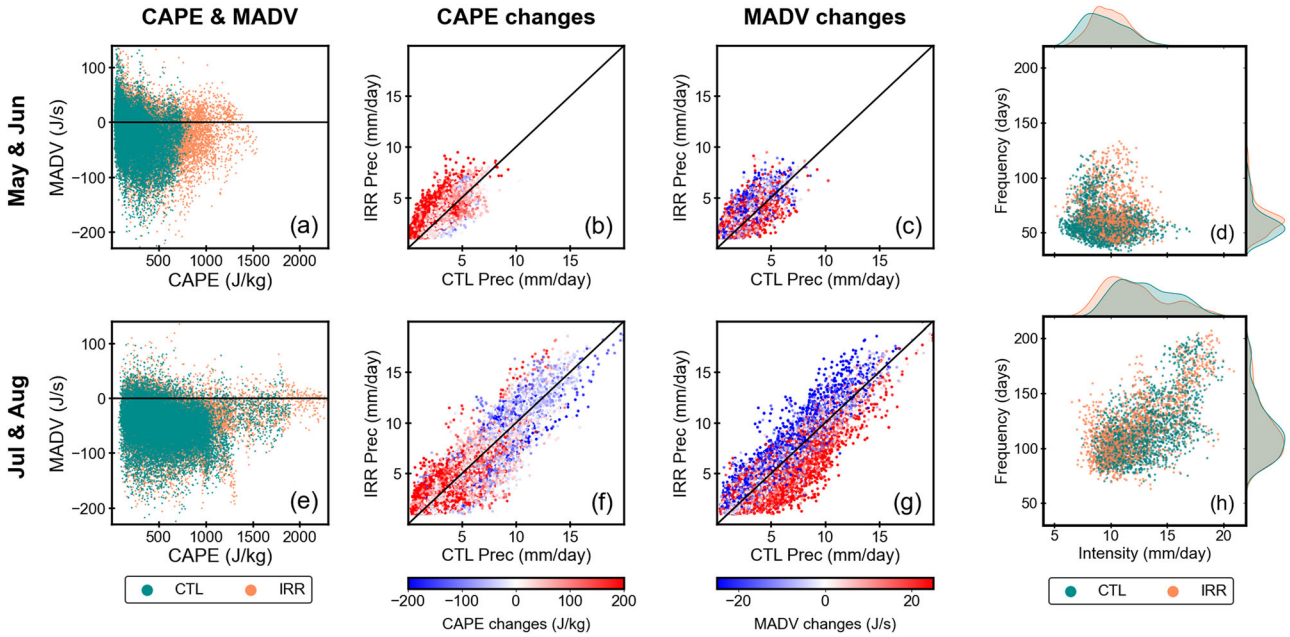

Fig. 8 | Relationships among CAPE, MADV, and precipitation. Each dot representing a monthly value of each land grid in the NCP for (**a**–**d**) May-Jun and (**e**–**h**) Jul-Aug. **a**, **d** CAPE and MADV in the CTL (green) and IRR (orange) experiment. **b**, **e** Precipitation amounts with colors representing changes in CAPE. **c**, **f** Precipitation amounts with colors representing changes in MADV. **d**, **g** Joint distribution of precipitation intensity and frequency where days with precipitation exceeding 1 mm are counted as rainy days.

heavy precipitation. The approximately equal distribution of dot colors on either side of the diagonal implies that changes in CAPE may not significantly affect precipitation variations, even at the individual precipitation level.

However, in Fig. 8c, g, most dots below the diagonal are associated with MADV increase, indicating the precipitation decrease in July and August is linked to greater vertical moisture divergence. Similarly, MADV decreases promote precipitation in most cases. Finally, there is a reduction in precipitation intensity, as evidenced by the leftward shift in the intensity distribution during July and August. However, the frequency remains unchanged, as the increase in CAPE is insufficient to trigger new precipitation, while the decrease in MADV does not completely stop the heavy rainfall. Overall, CAPE increases enhance both intensity and frequency in May and June, while MADV increases lead to reduced precipitation intensity in July and August.

Relationship of upper-troposphere and precipitation changes

Given the influence of CAPE and MADV on individual grids, we also seek to understand their effects on spatial patterns. Fig. S3 and Fig. 9 present the irrigation-induced differences for June, July, and August. For CAPE (Fig. S3 b, f, j) and MADV (Fig. S3 c, g, k), blue color ranges related to their potential enhancement of precipitation, while red signifies suppression. As expected, CAPE and MADV perform contrasting changes. The spatial pattern of CAPE increment generally resembles the irrigation pattern, whereas the spatial pattern of MADV decrement aligns more closely with precipitation variations observed in July and August, reinforcing the conclusion that MADV plays a more dominant role during these months.

Additionally, the precipitation decreases (Fig. 9a, e, i) in northern NCP is more evident during July, but extends southward to the entire NCP in August, while an increasing trend is observed in the southern part of the increasing region during both months. A similar pattern has been identified by Yang et al.[6]. Influenced by both moistening and stabilization effects, the relative changes in high-level water vapor content (QV) (Fig. 9b, f, j) not only reflect the distinct precipitation decrease in July and August compared to other months but also captures spatial details, such as the increment in northern part and decrement in southern part. This is further supported by the vertical cross section of water vapor at 115°E (Fig. 9c, g, k), where relatively substantial precipitation changes occur in all three months. A consistent increase in QV at low levels is accompanied by a decrease just above 850hPa, covering most of the NCP region. However, these low-level changes do not fully explain the spatial and monthly variations in precipitation response. Notably, QV changes around 200hPa may capture more about the temporal and spatial variations, especially the latitudinal precipitation, as illustrated in the bar charts (Fig. 9d, h, l).

To explain the vertical structure of QV changes, we also examine the vertical profiles of temperature and geopotential height (GH) in Fig. S4. There is a GH increase in near-surface level and the GH decrease in the whole mid to upper atmosphere, regardless of months. The irrigation-induced cooling is also confined to levels below 850 hPa, in contrast to the troposphere-wide cooling caused by crop expansion in northeast China[43]. This suggests that the GH reduction in the mid to high levels may not be directly driven by cooling. Instead, we hypothesize that changes in circulation patterns may play a more significant role. The circulation changes at different levels in June (Fig. 10) also indicate low-level divergence at 900 hPa, which disperses excess moisture outward. This process may trigger the wind convergence observed in upper levels. A cyclonic anomaly centered over the NCP land area at 700 hPa converges dry air, while it shifts northeast toward the ocean bay at 200 hPa, where it can gather moisture. In other words, the observed precipitation increases may not be fully linked to extra irrigation water but also the high-level moisture gathering driven by advection from remote areas due to the circulation changes.

To further prove this, we selected four extreme cases—two showing precipitation increases and two with decreases, one for July and one for August each—represented as red dots in Fig. 6. And Fig. 11 compares the changes in 200 hPa GH and the wind anomalies from these extreme cases, and Fig. S5 also provides the climatology mean with more cases highlighted in Fig. S6. Climatologically, there is 200hPa GH decreases in North China and Northeast China with cyclonic anomalies, correlating with the slight precipitation decrease in these regions, however, significant inter-annual variability is shown in the extreme cases (Fig. S5). Specifically, cases with notable precipitation increase are associated with slight GH decreases alongside weak cyclonic activity or strong GH increases with robust

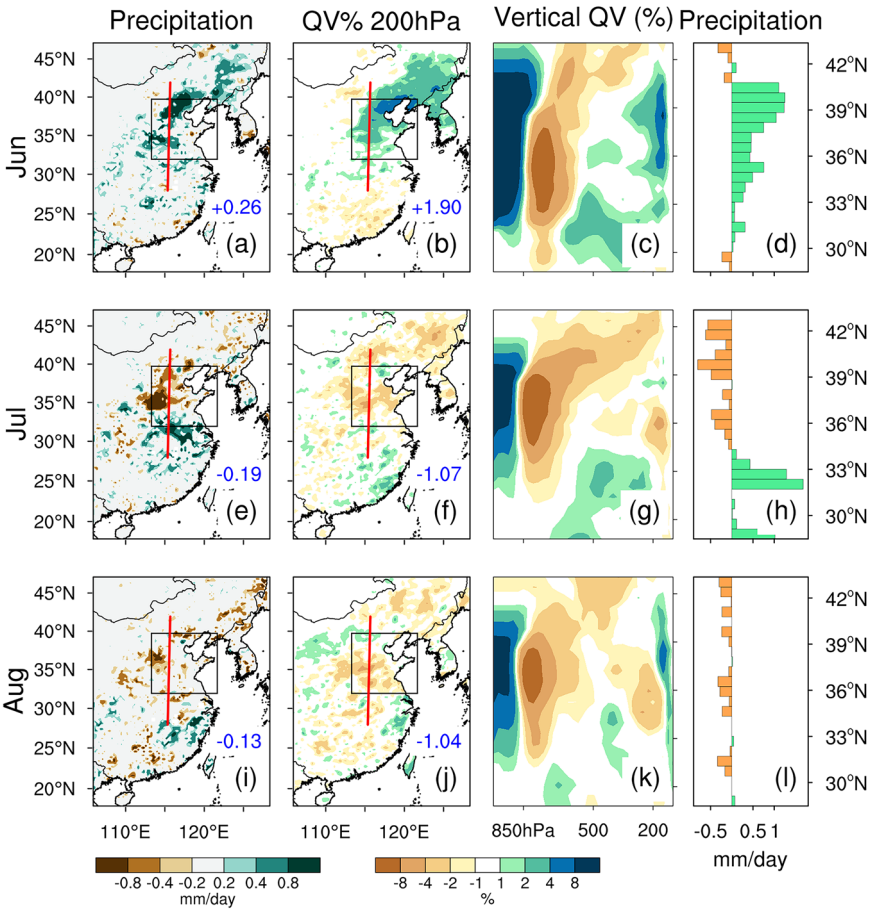

Fig. 9 | Relationship between irrigation-induced humidity changes and precipitation changes. Differences between CTL and IRR in **a**–**d** June, **e**–**h** July and **i**–**l** August. **a**, **e**, **i** Precipitation differences filtered by 70% consistent test (consistently increase or decrease for equals to or more than 7 out of the 10 years). **b**, **f**, **j** QV relative differences compared to CTL. **c**, **g**, **k** Relative changes in vertical structure of the QV cross section at 115°E. **d**, **h**, **l** Ground precipitation changes at the cross section at 115°E. The position of the cross section is indicated by the red bars. The vertical cut and corresponding precipitation at 115°E shares the same the latitudinal axis on the right side, while all other spatial plots share a different axis on the left. The numbers indicate spatial mean changes over NCP land grids.

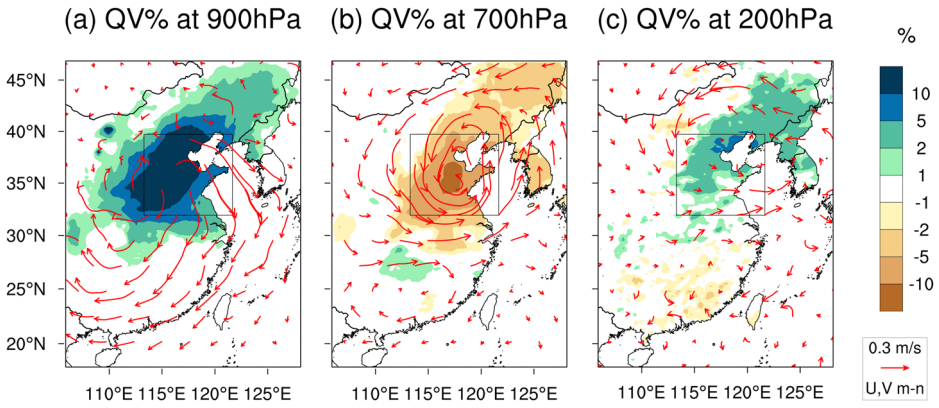

Fig. 10 | Irrigation-induced moisture transportation at different levels. The relative changes of water vapor and the wind anomaly at (**a**) 900 hPa, (**b**) 700 hPa and (**c**) 200 hPa in June.

anticyclonic conditions (Fig. 11 a, e, and c, g). In contrast, significant precipitation decreases consistently correlate with pronounced GH decreases and strong cyclonic anomalies, regardless of their regional centers, which may shift every year (Fig. 11b, f and d, h). This correlation is also evident in Fig. S6 with more extreme cases are tested. Moreover, Fig. S6 also shows that the cyclone centers coincide with areas of decreasing QV and precipitation.

Thus, we can infer that while irrigation introduces moisture, certain regions (e.g., North China) may be dominated by stabilization, leading to moisture transport to areas not dominated by anticyclones (e.g., South China), where it can result in precipitation. The geopotential height increase in the southern China also aligns with the non-convective precipitation increase found in Fig. 4, indicating irrigation may promote large-scale non-convective precipitation by shaping large circulation pattern. However, this guess need further proof since the magnitude of geopotential height changes and precipitation relative changes are too small. Among these extreme instances, we did not observe a clear relationship between irrigation forcing and the precipitation response. However, the relative changes in high-level QV maintained a strong proportionality with precipitation changes.

Discussion

Extensive and intensive irrigation practices have raised environmental concerns in the North China Plain (NCP), yet current studies reveal inconsistencies regarding irrigation-climate interactions. We have identified three primary deficiencies in existing climate models that contribute to these issues: (1) the omission of dynamic simulation for crops, (2) the absence of double cropping, and (3) the inappropriate parameters for crop and

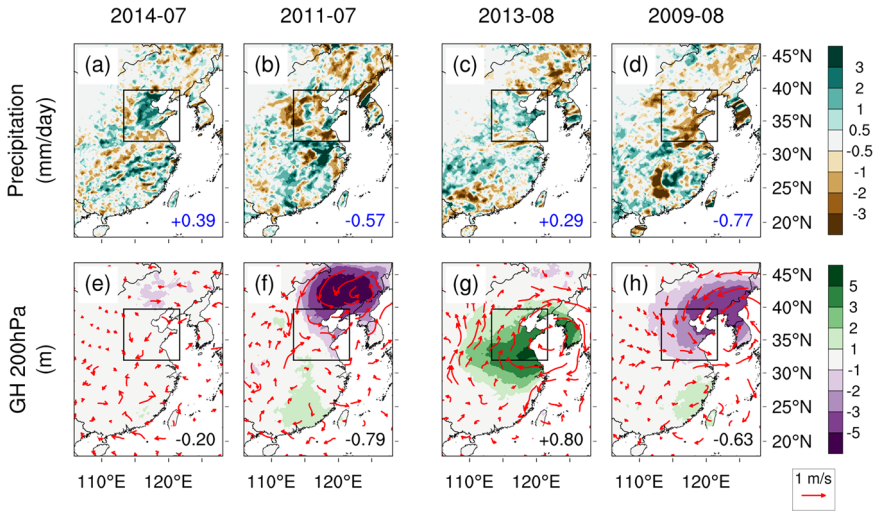

Fig. 11 | Precipitation variations and the 200 hPa GH changes with corresponding wind anomalies of climatology and extreme cases in July and August. a The greatest irrigation-induced increase in July among the 10-year experiments. **b** The greatest irrigation-induced decrease in July among the 10-year experiments. **c**, **d** are similar to (**a**, **b**) but for August. **e**–**h** Relative changes in 200hPa geopotential height and wind anomaly that are corresponding to (**a**–**d**). The numbers indicate spatial mean precipitation changes over NCP land grids (blue), and geopotential height changes over land grids in the whole domain (black numbers).

irrigation in the NCP region. Therefore, we employed an improved Noah-MP model specifically designed to address these deficiencies. The enhanced model demonstrates significant improvements in climate, crop, and irrigation simulation, providing a robust foundation for studying the irrigation impact.

Using the improved model, we first conduct an initial overview of the irrigation impact. Irrigation primarily induces cooling and humidification, subsequently producing both enhancement and suppression in precipitation; however, the overall enhancement predominates, leading to significant convective precipitation and total precipitation increases. Through temporal pattern analysis, we established that irrigation patterns result from a combination of precipitation, temperature, and crop rotation, which in turn influence back onto climate. Across all months, cooling is nearly proportional to irrigation forcing. Precipitation increases are significant and consistent during May and June, while decreases in July and August are insignificant and exhibit considerable inter-annual variability. This variability arises because, while irrigation promotes precipitation in some grids, the suppressive effects become more pronounced, particularly in July and August, leading to an overall decrease but inconsistent inter-annual changes.

To further investigate the competing effect, we employed CAPE as a representative of "enhancement" and MADV as a representative of "suppression". CAPE significantly increases in May and June, triggering new precipitation and intensifying existing rainfall. However, while CAPE increases are observable in light precipitation in July and August, insufficient water forcings and a more humid background diminish their significance and impact on precipitation patterns. Consequently, MADV controls precipitation changes in these two months. But MADV changes do not initiate new rainfall or completely halt existing rainfall, resulting in decreased intensity while maintaining frequency. Although the competing CAPE and MADV generally explain the distinctive precipitation responses in July-August compared to May-Jun, they fail to capture spatial details or the inter-annual variability. The analysis of vertical structure reveals that the spatial heterogeneity of precipitation changes is closely related to changes in high-level QV. This relationship may not be solely attributed to irrigation-induced additional moisture but also influenced by moisture advection from remote areas due to changes in circulation patterns. Furthermore, case studies of extreme events elucidate inter-annual discrepancies through anomalies in high-level GH and wind patterns. Thus, we can estimate the general changes of irrigation on precipitation using GH and wind patterns, and discern more localized details based on high-level QV patterns.

Our analysis of irrigation effects highlights the importance of addressing those identified model deficiencies. First, the inclusion of dynamic vegetation is essential, as evapotranspiration serves as a fundamental mechanism through which irrigation impacts climate. Second, the implementation of double cropping shows considerable potential in shaping irrigation practices in spring and early summer, influencing subsequent climatic responses. Third, the interactive irrigation-land-atmosphere feedback is clearly illustrated in Fig. 5, 6. The increase in precipitation during June is ~0.4 mm/day, accounting for about 20% of the irrigation amount for that month. This indicates that the two-way interactive irrigation model, rather than an offline simulation, could potentially reduce irrigation usage by about 20% because of the precipitation response. Additionally, our enhanced model incorporates feedback from irrigation cooling, resulting in reduced evaporation losses and improved irrigation efficiency. This feedback may also implicitly extend the crop growth period[22] and improve maize yield[44] compared to offline models.

Since the inter-annual variability in summer precipitation response is closely linked to 200 hPa GH and wind anomalies—common indices for measuring monsoonal activity[45–47]—we suspect that these responses are influenced by larger circulation patterns, such as the East Asian Summer Monsoon. Jeong et al.[48] suggest that variations in monsoon strength can produce differing precipitation responses to the transition from single-cropping to double-cropping. However, due to the limited spatial coverage and timespan of our study, we cannot further investigate this relationship between irrigation impact and monsoon, leaving this question open for future research.

Given the high-level GH changes are relatively minor compared to their original values, questions arise regarding whether surface irrigation can truly influence precipitation by altering the upper atmosphere. But similar to ours, Yang et al.[6] and Lee et al.[49] also found a decrease in high-level GH companying with cyclonic anomaly over the irrigated land, and their findings align also with ours in terms of the magnitude. Both studies argue that the easterly (or westerly) branch of the anomaly interacts with the prevailing westerly winds at 200 hPa, thereby undermining (or intensifying) the prevail upper-level westerly jet in the northern (or southern) regions of irrigation. In essence, this indicates a southward shift of the East Asian jet, which is generally recognized to increase precipitation over the Yangtze River Basin and decrease precipitation over the northern part[50–52]. Yang et al.[6] also highlighted a reduction in high-level cloud fraction and cloud water content due to irrigation. Further considering the spatial similarities between 200 hPa QV pattern and precipitation, as well as the inter-annual correlation of 200hPa wind anomalies and precipitation found in this study, we should acknowledge that high-level atmospheric changes, even if not the direct cause of summer precipitation changes, likely result from a combination of enhancing and suppressive factors, similar to precipitation itself. Thus, this leads to high correlations between the two. Conversely, while the low-level atmosphere is generally more affected by irrigation, it is also

influenced by other factors, resulting in a noisy pattern that obscures a direct relationship with precipitation

Throughout our research, we also identify that significant uncertainties could be raised from water forcings, including their quantity and timing. For instance, substantial discrepancies in water forcing likely contribute to disagreements in cooling responses, given the proportional relationship between cooling and water input. Among other RCM-based studies, we observed regional cooling ranges from 0.15 to 4 °C due to variations in irrigation seasons and water inputs. Additionally, any minor shifts in double-cropping rotation timing may affect the peak irrigation period. Although the improved model we employed made substantial efforts to calibrate irrigation amounts and validate rotation timing using satellite data, we remain cautious regarding the potential for significant uncertainties, and we recommend incorporating water sensitivity tests in future studies to quantify variability ranges. While we have noted model deficiencies as possible sources of disagreement in findings, the extent to which diverse conclusions arise with or without these deficiencies remains uncertain. Few studies have explored the potential climate variations caused by double-cropping[48], dynamic vegetation[7,53], and irrigation schemes[54,55]. More rigorous experiments that incorporate these elements can be conducted using this improved model in future research.

Lastly, while the model we adopted has significantly improved irrigation simulation, some deficiencies remain. In addition to the lack of spatial and temporal variability in crop parameters[22], the over-idealization of irrigation methods may also affect our findings on irrigation impacts. In reality, most regions utilize the 'Flooding' method[56], while our model simplifies irrigation to a fixed 'Drip' method, overlooking water loss due to evaporation and rapid drainage, and their subsequent climatic impacts[29]. Furthermore, farmers typically apply irrigation water only during critical stages of crop growth based on their experience and general assessments of soil moisture, but our irrigation schedule is set on a daily basis and heavily relies on water availability. Overall, while our model has improved, it still does not fully capture the complexities of realistic irrigation practices, primarily due to its limited ability to simulate precise vegetation and soil water dynamics compared to other offline agricultural and hydrological models. Therefore, addressing these limitations will be essential for advancing model development and enhancing the accuracy of irrigation simulations in future research.

Methods

Model introduction

The Noah-MP crop model, also known as WRF-Crop when integrated with WRF, was originally developed to simulate crop growth in two fields in the Central United States[26,57]. A dynamic irrigation scheme was later added to enhance crop management[58]. A fixed soil moisture threshold (SMCLIM) is defined as a value between the maximum soil moisture (SMCMAX, i.e., saturation) and minimum soil moisture (SMCMIN, i.e., wilting point), and the manageable availability deficit (MAD) is the parameter used to calibrate this threshold (Eq. 1). Subsequently, the model was applied at a regional scale across the Contiguous U.S. by transitioning MAD and other parameters from fixed values to state-specific variable values[23,59].

$$\mathrm{SMCLIM} = \mathrm{MAD} * \mathrm{SMCMAX} + (1 - \mathrm{MAD}) * \mathrm{SMCMIN}, \ \text{where } 0 \le \mathrm{MAD} \le 1 \quad (1)$$

Building on this foundation, Fan et al.[22] further improved the model to better study irrigation impacts in the NCP, aiming to fill the three model gaps, (1) the omission of dynamic simulation for crops, (2) the absence of double cropping, and (3) the inappropriate parameters for crop and irrigation in the NCP region, mentioned in the introduction.

First, improvements have been made for simulating dynamic vegetation. The default Noah-MP calculates crop growth rates with a particular sensitivity to weather, especially water availability, allowing for a more accurate representation of vegetation responses to varying irrigation levels. The water-sensitive growth rate influences the accumulation of LAI and Stem Area Index (SAI), which in turn affects albedo and energy budget[26]. The improved model also accounts for water-sensitive variations in vegetation fraction, another key variable for energy and water partitioning. While the original model used a fixed vegetation fraction of 95% for all grids at all times (Eq. 2), the enhanced model correlates vegetation fraction with LAI and SAI using empirical relationships (Eq. 3), enabling spatial and temporal variability in vegetation. Additionally, the crop calendar is calculated based on GDD accumulation, integrating the extended crop season induced by irrigation cooling into the simulation.

$$\text{Original FVEG} = 0.95 \quad (2)$$

$$\text{Adjusted FVEG} = 0.75 - 0.5 \times e^{(-0.52 \times (\mathrm{LAI}+\mathrm{SAI}))} \quad (3)$$

Second, the improved model also incorporates the double-cropping rotations into the model, as well as the winter and spring irrigation which is related to winter cropping season. Winter wheat and summer maize, which are the most prevalent crop types, are rotated over the double-cropping region, with spring maize in the single-cropping region. The introduction of winter wheat may trigger excessive winter irrigation due to dry soil conditions, which can waste water and harm crops. Thus, a soil temperature check (i.e., if the averaged soil temperature in the past 24 h is greater than 5 °C) is included in the improved model to enhance water efficiency and prevent irrigation-induced frozen soil (Eq. 5). To align with common agricultural practices[6,60], the improved model specifies irrigation from 6 A.M. to 10 A.M. local time during the crop season, calculated solely by the crop model, thus better defining both the crop and irrigation seasons. And the irrigation amount is also correlated with the irrigation fraction (Eq. 5) instead of a fixed value (Eq. 4).

$$\text{Default Irrigation Amount} = \int (\mathrm{SMCLIM} - \mathrm{SMCAVL}) * 0.95 \quad (4)$$

$$\text{Adjusted Irrigation Amount} = \begin{cases} \int (\mathrm{SMCLIM} - \mathrm{SMCAVL}) * \mathrm{IRRFRA} & (\text{when } T_{soil24h} \ge 5^{\circ}\mathrm{C}) \\ 0 & (\text{when } T_{soil24h} < 5^{\circ}\mathrm{C}) \end{cases} \quad (5)$$

Lastly, rather than relying on default crop parameters derived from the central U.S., the model was recalibrated and validated using NCP observations. Spatially varied planting date and harvest date were redefined based on satellite-based post-processed dataset[61]. Other crop calendar components, such as the heading and physiological maturity dates, were validated to confirm the appropriateness of the planting and harvest dates. After settling down the crop calendar, photosynthesis rates and carbon allocations were recalibrated to accurately capture leaf and stem biomass at two agricultural stations: Yucheng in the double-cropping region and Shenyang in the single-cropping region. Following calibration at these stations, the parameters were applied to the regional scale, and the spatial patterns of monthly LAI and vegetation fraction were validated to assess their suitability across the entire NCP. The model now captures two annual vegetation peaks, with spatial patterns closely mirroring those observed in satellite data[22]. Finally, similar to the state-specific parameters in the US, province-level calibration of irrigation thresholds (i.e., MAD) was conducted, improving the spatial distribution of irrigation and aligning it more closely with observed irrigation amounts. All the required inputs and calibrated parameters are listed in Fan et al.[22].

In conclusion, this model ensures that crop growth, irrigation, and the background climate are all dynamically interactive, capturing both direct and indirect irrigation impacts more comprehensively. All modifications and parameter recalibrations were specifically designed for the NCP region, enhancing the model's potential for studying irrigation impacts in our targeted domain.

Model domain and experiment design

This study utilizes the Advanced Research WRF Model (version 4.5) with a horizontal resolution of 27 km, 38 vertical atmospheric layers and 4 soil layers. The physical parameterization options include the WRF double-moment 5-class microphysics scheme[62], the Rapid Radiative Transfer Model for longwave radiation[63], the Dudhia shortwave radiation scheme[64], the Yonsei University planetary boundary layer scheme[65], the scale-aware New Simplified Arakawa-Schubert scheme[66,67], and the Noah-MP land surface model[68], which is coupled with the improved crop and irrigation schemes[22].

To ensure consistency, we adopt the same domain setting used for developing the model. The model domain, centered on the NCP, encompasses a significant portion of irrigated cropland (Fig. 1). It is a single domain, and the inner black box serves only to highlight the NCP region. The topography was initially sourced from the United States Geological Survey. Crop model is activated when either "Croplands" or "Cropland/Natural Vegetation Mosaics" account for the majority of the grid based on MODIS (Moderate-resolution Imaging Spectroradiometer) land-use classification. There may be an overestimation of the cropping region due to the low reliability of MODIS land cover data in China, but primarily affects the boundaries rather than heavily irrigated areas that we focus on.

With this domain setting, all experiments span a 10-year period from 2005 to 2014, incorporating a nine-month spin-up beginning in March 2004 to ensure model initialization. WRF experiments are performed under two scenarios: one without irrigation (CTL) and another with irrigation (IRR), calibrated using the 2005 statistical irrigation data[22]. Since the default model may not reproduce reasonable crop growth and irrigation application[22], both experiments are conducted using the improved model (i.e., with double-cropping and calibrated crop parameters). The only difference between the experiments is the activation of irrigation, which can explicitly show the irrigation-induced climate changes. Initial and lateral boundary conditions are derived from the 6-h ERA-Interim reanalysis dataset[69].

Observation data

For temperature and precipitation, we use CN05 dataset with 0.25 degree resolution[4]. LAI dataset is derived from MODIS satellite product and later post-processed by Sun Yat-sen University[21]. Crop yield data comes from the GAEZ + _2015[70], while irrigation estimates are based on province-based statistics from National Bureau of Statistics of China[22,71]. Runoff data is obtained from the hydrological model, validated with station observations across various basins[72]. Regardless of the original resolution, all observations are interpolated to the model grids, as some analyses require spatial averaging over land, cropping, or double-cropping regions, which are defined by the model grid. All datasets have the same timespan as our experiments, except for the crop yield is only for 2010. We collectively refer to all of these data as observations in this study.

Data availability

The source code for a dynamic double-cropping model with interactive irrigation is freely available at https://doi.org/10.5281/zenodo.10729554. The climatology temperature and precipitation are retrieved from the CN05.1 dataset. It is produced by Cold and Arid Regions Science Data Center and is available at https://doi.org/10.3972/westdc.002.2014.db. The LAI dataset was initially from Sun Yat-sen University, shown at http://globalchange.bnu.edu.cn/research. The cropping pattern is defined by ChinaCP, available at https://doi.org/10.6084/m9.figshare.14936052. Runoff data is obtained from the ensemble mean of VIC model, which is available at https://data.tpdc.ac.cn/zh-hans/data/70a3ad6b-9847-476d-a11e-a493d6c31af1. The yield data is provided by GAEZ + _2015 and it's freely available from https://doi.org/10.7910/DVN/XGGJAV. Validation irrigation amount is estimated based on the province-based statistical dataset in China Statistical Yearbook, with access from https://www.stats.gov.cn/sj/ndsj/2005/indexeh.htm.

Received: 31 December 2024; Accepted: 23 April 2025;
Published online: 06 June 2025

References

1. Bonfils, C. & Lobell, D. Empirical evidence for a recent slowdown in irrigation-induced cooling. *Proc. Natl. Acad. Sci. USA.* **104**, 13582–13587 (2007).
2. Foley, J. A. et al. Solutions for a cultivated planet. *Nature* **478**, 337–342 (2011).
3. Qiu, B. et al. Maps of cropping patterns in China during 2015–2021. *Sci. Data* **9**, 479 (2022).
4. Wu, J. & Gao, X.-Jie A gridded daily observation dataset over China region and comparison with the other datasets. *Chin. J. Geophys.* **56**, 1102–1111 (2013).
5. Siebert, S. et al. Historical Irrigation Dataset (HID). MyGeoHUB. https://doi.org/10.13019/M20599 (2013).
6. Yang, B., Zhang, Y., Qian, Y., Tang, J. & Liu, D. Climatic effects of irrigation over the Huang-Huai-Hai Plain in China simulated by the weather research and forecasting model. *J. Geophys. Res. Atmos.* **121**, 2246–2264 (2016).
7. Wu, L., Feng, J. & Miao, W. Simulating the impacts of irrigation and dynamic vegetation over the North China Plain on Regional Climate. *J. Geophys. Res. Atmos*. https://doi.org/10.1029/2017JD027784. (2018).
8. Kang, S. & Eltahir, E. A. B. Impact of irrigation on regional climate over Eastern China. *Geophys. Res. Lett.* **46**, 5499–5505 (2019).
9. Liu, J., Jin, J. & Niu, G. Effects of irrigation on seasonal and annual temperature and precipitation over China simulated by the WRF model. *J. Geophys. Res. Atmos.* **126**, e2020JD034222 (2021).
10. Cui, F. et al. Interplay between urbanization and irrigation on summer climate in the Huang-Huai-Hai Plain, China. *J. Geophys. Res. Atmos.* **127**, e2021JD036053 (2022).
11. Fan, Y., Im, E.-S., Lan, C.-W. & Lo, M.-H. An increase in precipitation driven by irrigation over the North China Plain based on RegCM and WRF simulations. *J. Hydrometeorol*. https://doi.org/10.1175/JHM-D-22-0131.1 (2023).
12. Wu, J., Han, Z.-Y., Gao, X.-J. & Liu, Z.-J. Climatic impacts induced by winter wheat irrigation over North China simulated by the nonhydrostatic RegCM4.7. *Adv. Clim. Change Res.* **15**, 197–210 (2024).
13. Xie, T. et al. Influence of the North Atlantic sea surface temperature on decadal variability of the July precipitation in north China. *Int. J. Climatol.* **43**, 964–978 (2023).
14. Sorooshian, S., Li, J., Hsu, K. & Gao, X. How significant is the impact of irrigation on the local hydroclimate in California's Central Valley? Comparison of model results with ground and remote-sensing data. *J. Geophys. Res.* **116**, D06102 (2011).
15. Leng, G. et al. Modeling the effects of irrigation on land surface fluxes and states over the conterminous United States: sensitivity to input data and model parameters: effects of irrigation over conus. *J. Geophys. Res. Atmos.* **118**, 9789–9803 (2013).
16. Mehboob, M. S. et al. Projection of vegetation impacts on future droughts over West Africa using a coupled RegCM-CLM-CN-DV. *Clim. Change* **163**, 653–668 (2020).
17. Kim, Y. & Wang, G. Soil moisture-vegetation-precipitation feedback over North America: its sensitivity to soil moisture climatology: SM-V-P sensitivity to soil moisture climatology. *J. Geophys. Res*. **117**, n/a-n/a (2012).
18. Wang, G. & Eltahir, E. A. B. Role of vegetation dynamics in enhancing the low-frequency variability of the Sahel rainfall. *Water Resour. Res*. **36**, 1013–1021 (2000).
19. Wang, G., Sun, S. & Mei, R. Vegetation dynamics contributes to the multi-decadal variability of precipitation in the Amazon region: vegetation dynamics and amazon rainfall. *Geophys. Res. Lett*. **38**, n/a-n/a (2011).
20. Harding, K. J., Twine, T. E. & Lu, Y. Effects of dynamic crop growth on the simulated precipitation response to irrigation. *Earth Interact.* **19**, 1–31 (2015).

21. Yuan, H., Dai, Y. & Li, S. Reprocessed MODIS Version 6 Leaf Area Index data sets for land surface and climate modelling. (2020).
22. Fan, Y., Yang, Z., Lo, M.-H., Hur, J. & Im, E.-S. Applying double cropping and interactive irrigation in the North China Plain using WRF4.5. *Geosci. Model Dev.* **17**, 6929–6947 (2024).
23. Zhang, Z. et al. Joint Modeling of Crop and Irrigation in the central United States Using the Noah-MP Land Surface Model. *J. Adv. Model. Earth Syst*. **12**, (2020).
24. Yao, Y. et al. Implementation and evaluation of irrigation techniques in the community land model. *J. Adv. Model. Earth Syst.* **14**, e2022MS003074 (2022).
25. Qian, Y. et al. Neglecting irrigation contributes to the simulated summertime warm-and-dry bias in the central United States. *npj Clim. Atmos. Sci.* **3**, 31 (2020).
26. Liu, X., Chen, F., Barlage, M., Zhou, G. & Niyogi, D. Noah-MP-Crop: introducing dynamic crop growth in the Noah-MP land surface model: Noah-MP-Crop. *J. Geophys. Res. Atmos.* **121**, 13,953–13,972 (2016).
27. Seo, H. & Kim, Y. Role of remotely sensed leaf area index assimilation in eco-hydrologic processes in different ecosystems over East Asia with Community Land Model version 4.5 – Biogeochemistry. *J. Hydrol.* **594**, 125957 (2021).
28. Wang, Y. et al. Responses of summer mesoscale convective systems to irrigation over the North China Plain based on convection-permitting model simulations. *Environ. Res. Commun*. https://doi.org/10.1088/2515-7620/ad78ba (2024).
29. Yuan, T. et al. Effects of different irrigation methods on regional climate in North China Plain: a modeling study. *Agric. Meteorol.* **342**, 109728 (2023).
30. Gao, Y., Hsu, P.-C., Che, S., Yu, C. & Han, S. Origins of intraseasonal precipitation variability over North China in the rainy season. *J. Clim.* **35**, 6219–6236 (2022).
31. Huber, D., Mechem, D. & Brunsell, N. The effects of great plains irrigation on the surface energy balance, regional circulation, and precipitation. *Climate* **2**, 103–128 (2014).
32. Li, J. et al. Impacts of large-scale urbanization and irrigation on summer precipitation in the Mid-Atlantic region of the United States. *Geophys. Res. Lett*. **49**, (2022).
33. Im, E.-S., Marcella, M. P. & Eltahir, E. A. B. Impact of potential large-scale irrigation on the West African monsoon and its dependence on location of irrigated area. *J. Clim.* **27**, 994–1009 (2014).
34. Pei, L. et al. Effects of irrigation on summer precipitation over the United States. *J. Clim.* **29**, 3541–3558 (2016).
35. Lo, M.-H. et al. Intense agricultural irrigation induced contrasting precipitation changes in Saudi Arabia. *Environ. Res. Lett.* **16**, 064049 (2021).
36. Lee, E. et al. Effects of irrigation and vegetation activity on early Indian summer monsoon variability. *Int. J. Climatol.* **29**, 573–581 (2009).
37. DeAngelis, A. et al. Evidence of enhanced precipitation due to irrigation over the Great Plains of the United States. *J. Geophys. Res.* **115**, D15115 (2010).
38. Alter, R. E., Douglas, H. C., Winter, J. M. & Eltahir, E. A. B. Twentieth century regional climate change during the summer in the central United states attributed to agricultural intensification. *Geophys. Res. Lett.* **45**, 1586–1594 (2018).
39. Yang, Z. et al. Irrigation impact on water and energy cycle during dry years over the united states using convection-permitting WRF and a dynamical recycling model. *J. Geophys. Res. Atmos.* **124**, 11220–11241 (2019).
40. Yang, Z. et al. Understanding irrigation impacts on low-level jets over the Great Plains. *Clim. Dyn.* **55**, 925–943 (2020).
41. Chou, C. & Lan, C.-W. Changes in the annual range of precipitation under global warming. *J. Clim.* **25**, 222–235 (2012).
42. Chen, C.-C. et al. Thermodynamic and dynamic responses to deforestation in the maritime continent: a modeling study. *J. Clim.* **32**, 3505–3527 (2019).
43. He, Y., Lee, E. & Mankin, J. S. Seasonal tropospheric cooling in Northeast China associated with cropland expansion. *Environ. Res. Lett.* **15**, 034032 (2020).
44. Han, L. & Leng, G. Global irrigation cooling benefits for maize yield: the spatial–temporal patterns and possible mechanisms. *J. Hydrol.* **655**, 132961 (2025).
45. Zhu, C., Lee, W., Kang, H. & Park, C. A proper monsoon index for seasonal and interannual variations of the East Asian monsoon. *Geophys. Res. Lett.* **32**, 2004GL021295 (2005).
46. Sun, L., Shen, B., Sui, B. & Huang, B. The influences of East Asian Monsoon on summer precipitation in Northeast China. *Clim. Dyn.* **48**, 1647–1659 (2017).
47. Chen, W. & Guan, Z. A joint monsoon index for East Asian–Australian monsoons during boreal summer. *Atmos. Sci. Lett.* **18**, 403–408 (2017).
48. Jeong, S.-J. et al. Effects of double cropping on summer climate of the North China Plain and neighbouring regions. *Nat. Clim. Change* **4**, 615–619 (2014).
49. Lee, E., Sacks, W. J., Chase, T. N. & Foley, J. A. Simulated impacts of irrigation on the atmospheric circulation over Asia. *J. Geophys. Res.* **116**, D08114 (2011).
50. Liang, X. & Wang, W. Associations between China monsoon rainfall and tropospheric jets. *Q. J. R. Meteorol. Soc.* **124**, 2597–2623 (1998).
51. Lu, R. Associations among the components of the East Asian Summer Monsoon System in the Meridional direction. *J. Meteorol. Soc. Jpn. Ser. II* **82**, 155–165 (2004).
52. Wang, T. et al. Anthropogenic agent implicated as a prime driver of shift in precipitation in eastern China in the late 1970s. *Atmos. Chem. Phys.* **13**, 12433–12450 (2013).
53. Shi, Y., Yu, M., Erfanian, A. & Wang, G. Modeling the dynamic vegetation–climate system over China using a coupled regional model. *J. Clim.* **31**, 6027–6049 (2018).
54. Sorooshian, S., Li, J., Hsu, K. & Gao, X. Influence of irrigation schemes used in regional climate models on evapotranspiration estimation: results and comparative studies from California's Central Valley agricultural regions. *J. Geophys. Res.* **117**, 2011JD016978 (2012).
55. Sorooshian, S., AghaKouchak, A. & Li, J. Influence of irrigation on land hydrological processes over California. *J. Geophys. Res. Atmos*. **119**, (2014).
56. Jägermeyr, J. et al. Water savings potentials of irrigation systems: global simulation of processes and linkages. *Hydrol. Earth Syst. Sci.* **19**, 3073–3091 (2015).
57. He, C. et al. *The Community Noah-MP Land Surface Modeling System Technical Description Version 5.0* (2023).
58. Valayamkunnath, P. Dynamic Irrigation Management for NoahMP. (NCAR, 2020).
59. Xu, X. et al. Lessons learned from modeling irrigation from field to regional scales. *J. Adv. Model. Earth Syst.* **11**, 2428–2448 (2019).
60. Ozdogan, M., Rodell, M., Beaudoing, H. K. & Toll, D. L. Simulating the effects of irrigation over the united states in a land surface model based on satellite-derived agricultural data. *J. Hydrometeorol.* **11**, 171–184 (2010).
61. Luo, Y., Zhang, Z., Chen, Y., Li, Z. & Tao, F. ChinaCropPhen1km: a high-resolution crop phenological dataset for three staple crops in China during 2000–2015 based on leaf area index (LAI) products. *Earth Syst. Sci. Data* **12**, 197–214 (2020).
62. Hong, S.-Y., Dudhia, J. & Chen, S.-H. A revised approach to ice microphysical processes for the bulk parameterization of clouds and precipitation. *Mon. Wea. Rev.* **132**, 103–120 (2004).
63. Mlawer, E. J., Taubman, S. J., Brown, P. D., Iacono, M. J. & Clough, S. A. Radiative transfer for inhomogeneous atmospheres: RRTM, a validated correlated-k model for the longwave. *J. Geophys. Res.* **102**, 16663–16682 (1997).
64. Dudhia, J. Numerical study of convection observed during the winter monsoon experiment using a mesoscale two-dimensional model. *J. Atmos. Sci.* **46**, 3077–3107 (1989).

65. Hong, S.-Y., Noh, Y. & Dudhia, J. A new vertical diffusion package with an explicit treatment of entrainment processes. *Mon. Weather Rev.* **134**, 2318–2341 (2006).
66. Han, J. & Pan, H.-L. Revision of convection and vertical diffusion schemes in the NCEP global forecast system. *Weather Forecast.* **26**, 520–533 (2011).
67. Kwon, Y. C. & Hong, S.-Y. A mass-flux cumulus parameterization scheme across gray-zone resolutions. *Mon. Weather Rev.* **145**, 583–598 (2017).
68. Ek, M. B. et al. Implementation of Noah land surface model advances in the National Centers for Environmental Prediction operational mesoscale Eta model. *J. Geophys. Res.* **108**, 2002JD003296 (2003).
69. Dee, D. P. et al. The ERA-Interim reanalysis: configuration and performance of the data assimilation system. *Q. J. R. Meteorol. Soc.* **137**, 553–597 (2011).
70. Grogan, D., Frolking, S., Wisser, D., Prusevich, A. & Glidden, S. Global gridded crop harvested area, production, yield, and monthly physical area data circa 2015. *Sci. Data* **9**, 15 (2022).
71. National Bureau of Statistics of China. *China Statistical Yearbook*. http://www.stats.gov.cn/tjsj/ndsj/2005/indexeh.htm (National Bureau of Statistics of China, 2005).
72. Zhou, J. et al. Projection of China's future runoff based on the CMIP6 mid-high warming scenarios. *Sci. China Earth Sci.* **66**, 528–546 (2023).

Acknowledgements

This study was supported by the "Research Program for Agricultural Science & Technology Development (Project No. RS-2024-00399847)", National Institute of Agricultural Sciences, Rural Development Administration, Republic of Korea. Additionally, Im E.-S. was supported by the Theme-based Research Scheme (T31-603/21-N) and General Research Fund (GRF16308722), which were funded by the Research Grants Council (RGC) of Hong Kong. The contribution of Zhao Yang in this study is supported by the Office of Science of the U.S. Department of Energy (DOE) as part of the Atmospheric System Research (ASR) program through the Integrated Cloud, Land-surface, and Aerosol System Study (ICLASS) Science Focus Area via Grant KP1701000/57131. The authors thank HKUST Fok Ying Tung Research Institute and National Supercomputing Center in Guangzhou Nansha Sub-center for providing high performance computational resources.

Author contributions

Y.F. and E.I. conceptualized the idea. Y.F. performed the experiment and wrote the manuscript draft. All authors reviewed and edited the manuscript.

Competing interests

The authors declare no competing interests.

Additional information

Supplementary information The online version contains supplementary material available at https://doi.org/10.1038/s41612-025-01063-3.

Correspondence and requests for materials should be addressed to Yuwen Fan or Eun-Soon Im.